JPn Neuroscience

The Journal of Physiology

*J Physiol* 594.1 (2016) pp 223–237



# Deficiency of GABAergic synaptic inhibition in the Kölliker–Fuse area underlies respiratory dysrhythmia in a mouse model of Rett syndrome

Ana Paula Abdala[1], Marie A. Toward[1], Mathias Dutschmann[2], John M. Bissonnette[3] and Julian F. R. Paton[1]

[1] *School of Physiology and Pharmacology, Medical Sciences Building, University of Bristol, Bristol BS8 1TD, UK*
[2] *Florey Institute of Neuroscience and Mental Health, University of Melbourne, Gate 11, Royal Parade, Victoria 3052, Australia*
[3] *Department of Obstetrics and Gynecology, Oregon Health and Science University, Portland, OR 97239, USA*

**Key points**

- Life threatening breathing irregularity and central apnoeas are highly prevalent in children suffering from Rett syndrome.
- Abnormalities in inhibitory synaptic transmission have been associated with the physiopathology of this syndrome, and may underlie the respiratory disorder.
- In a mouse model of Rett syndrome, GABAergic terminal projections are markedly reduced in the Kölliker–Fuse nucleus (KF) in the dorsolateral pons, an important centre for control of respiratory rhythm regularity.
- Administration of a drug that augments endogenous GABA localized to this region of the pons reduced the incidence of apnoea and the respiratory irregularity of Rett female mice. Conversely, the respiratory disorder was recapitulated by blocking GABAergic transmission in the KF area of healthy rats.
- This study helps us understand the mechanism for generation of respiratory abnormality in Rett syndrome, pinpoints a brain site responsible and provides a clear anatomical target for the development of a translatable drug treatment.

**Abstract** Central apnoeas and respiratory irregularity are a common feature in Rett syndrome (RTT), a neurodevelopmental disorder most often caused by mutations in the methyl-CpG-binding protein 2 gene (*MECP2*). We used a MECP2 deficient mouse model of RTT as a strategy to obtain insights into the neurobiology of the disease and into mechanisms essential for respiratory rhythmicity during normal breathing. Previously, we showed that, systemic administration of a GABA reuptake blocker in MECP2 deficient mice markedly reduced the occurrence of central apnoeas. Further, we found that, during central apnoeas, post-inspiratory drive (adductor motor) to the upper airways was enhanced in amplitude and duration in *Mecp2* heterozygous female mice. Since the pontine Kölliker–Fuse area (KF) drives post-inspiration, suppresses inspiration, and can reset the respiratory oscillator phase, we hypothesized that synaptic inhibition in this area is essential for respiratory rhythm regularity. In this study, we found that: (i) *Mecp2* heterozygous mice showed deficiency of GABA perisomatic bouton-like puncta and processes in the KF nucleus; (ii) blockade of GABA reuptake in the KF of RTT mice reduced breathing irregularity; (iii) conversely, blockade of $GABA_A$ receptors in the KF of healthy rats mimicked the RTT respiratory phenotype of recurrent central apnoeas and prolonged post-inspiratory activity. Our results show that reductions in synaptic inhibition within the KF induce rhythm irregularity whereas boosting GABA transmission reduces respiratory arrhythmia in a murine model of RTT. Our data suggest that manipulation of synaptic inhibition in KF may be a clinically important strategy for alleviating the life threatening respiratory disorders in RTT.



DOI: 10.1113/JP270966

(Received 21 May 2015; accepted after revision 23 October 2015; first published online 28 October 2015)
**Corresponding author**: A. P. Abdala: School of Physiology and Pharmacology, Medical Sciences Building, University of Bristol, Bristol BS8 1TD, UK. Email: ana.abdala@bristol.ac.uk

**Abbreviations** 5N, motor trigeminal nucleus; A7, facial motor nucleus; CV, coefficient of variation; cVN, vagus nerve; DLL, dorsal nucleus of the lateral lemniscus; eGFP, enhanced green fluorescent protein; FOV, field of view; GAD, glutamic acid decarboxylase; IC, inferior colliculus; KF, Kölliker–Fuse area; KF-nu, Kölliker–Fuse nucleus; LPB, lateral parabrachial nuclei; MECP2, methyl-CpG-binding protein 2; *MECP2* or *Mecp2*, methyl-CpG-binding protein 2 gene (human and mouse, respectively); MECP2ir, MECP2 immuno-reactive; MPB, medial parabrachial nucleus; PAG, periaqueductal grey; PN, phrenic nerve; post-I, post-inspiration; RTT, Rett syndrome; scp, superior cerebellar peduncle; Su5, supratrigeminal nucleus; $T_E$, expiratory duration; $T_I$, inspiratory duration; $T_{TOT}$, total respiratory period; VIAAT, vesicular inhibitory amino acid transporter; XII, hypoglossal nerve.

## Introduction

Rett syndrome (RTT) is an autism spectrum disorder caused by mutations in the gene that encodes the nuclear protein methyl-CpG-binding protein 2 (MECP2). As *MECP2* is X-linked, the syndrome is seen primarily in females, due to high lethality in males. Amongst other symptoms, it features frequent apnoeas, breathing irregularities and periodic breathing (Lugaresi *et al.* 1985). The breathing impairment can be life-threatening and patients show a mixture of obstructive and central apnoeas (Carotenuto *et al.* 2012). In a mouse model of RTT, we and others demonstrated that excess expiratory motor output in early expiration, i.e. post-inspiration (post-I), characterizes the respiratory abnormality in both males (Stettner *et al.* 2007) and females (Abdala *et al.* 2010). Building on earlier reports that showed disturbances in GABAergic transmission in RTT models (Medrihan *et al.* 2008), we found that systemic administration of a GABA reuptake blocker significantly reduced the incidence of apnoeas and restored regularity to the breathing cycle.

In the present study, we explored the role of the pontine Kölliker–Fuse area (KF) in generating the respiratory impairment in RTT. The Kölliker–Fuse nucleus (KF-nu) and discrete parabrachial nuclei (medial, extreme-lateral and lateral-crescent) are the main regions involved in respiratory control in the parabrachial complex, and as per Dutschmann & Dick (2012) we will simply refer to them as the KF area (or KF). The KF provides essential drive for post-I, suppresses inspiration and can reset the respiratory oscillator phase (Moerschel & Dutschmann, 2009). It contains laryngeal post-inspiratory premotor neurons involved in the regulation of upper airway (Dutschmann & Herbert, 2006). In fact, studies in *Mecp2* null males showed active closure of the upper airways during apnoeas (Voituron *et al.* 2010). Given the evidence for disruption in GABAergic transmission in the brainstem (Medrihan *et al.* 2008), we hypothesized that deficient synaptic inhibition in the KF underlies the exacerbation in post-inspiratory drive and consequent respiratory irregularity in a mouse model of RTT. To reveal the anatomical substrate for this deficiency, we compared the number of GABA expressing perisomatic bouton-like structures on KF nucleus neurones in double transgenic mice expressing enhanced green fluorescent protein (eGFP) under the control of the glutamic acid decarboxylase 67 ($GAD_{67}$) promoter for both *Mecp2*$^{+/+}$ and *Mecp2*$^{+/-}$ females. We also compared cell-autonomous effects of protein deletion within *Mecp2*$^{+/-}$ tissue. Additionally, we postulated that if the mechanism for generation of respiratory irregularities in MECP2 deficient females involves deficits of GABA synaptic transmission in the KF, then augmenting endogenous GABA transmission in this area would rescue the respiratory phenotype. To test this, we microinjected a GABA reuptake blocker directly into the KF parenchyma of *Mecp2*$^{+/-}$ females to increase the availability of endogenously released GABA. Conversely, if loss of GABA synaptic transmission in the KF is sufficient to generate the respiratory irregularities in *Mecp2*$^{+/-}$ females, then mimicking this deficiency by blocking $GABA_A$ receptors in the KF of wild-type rats should generate an RTT-like respiratory phenotype. As a proof-of-concept, we microinjected a $GABA_A$ receptor antagonist directly into the KF parenchyma of rats, to mimic a local deficit of GABAergic synaptic transmission in a different mammalian species.

## Methods

### Animals

The experiments were performed according to the UK Home Office's Animals (Scientific Procedures) Act (1986) and approved by the University of Bristol ethics review committee. The *in situ* experiments in mice were performed in B6.129P2(C)-*Mecp2*$^{tm1.1Bird}$/J (stock number: 003890, The Jackson Laboratory, ME, USA) heterozygous females ($n = 7$) and in wild-type littermates ($n = 10$) aged 14 ± 1 months. These mice were bred on a C57BL6/J background. The *in situ* experiments in rats were performed in male Wistar rats (Harlan Laboratories, UK) at 21–27 days of age ($n = 8$).

Double transgenic heterozygous *Mecp2*$^{+/-}$ female mice carrying a $GAD_{67}$-eGFP transgene (*Mecp2*$^{+/-}$/$GAD_{67}$-EGFP, $n = 2$) and *Mecp2*$^{+/+}$/$GAD_{67}$-eGFP littermates

($n$ = 2, 15.5 ± 0.3 months of age) were generated by crossing males that were heterozygous for this transgene (CB6-Tg(GAD1-eGFP)G42zih/J, stock number: 007677, The Jackson Laboratory) with *Mecp2*$^{tm1.1Bird}$ heterozygous females. These males were on a mixed C57BL6/J, CB6F1/J background. In this strain, the eGFP transgene is selectively expressed in the calcium-binding protein parvalbumin (PV)-expressing neurones, including dendrites, soma, axons and especially bouton-like puncta (Chattopadhyaya *et al.* 2004). Parvalbumin expressing GABAergic neurones are abundant in key brainstem areas, including the ventrolateral medulla (Alheid *et al.* 2002), making this strain useful for the characterization of perisomatic innervation in respiratory nuclei. For ease-of-read henceforth we will refer to the labelled $GAD_{67}$-PV-eGFP-expressing neurones, projections and bouton-like structures as simply $GAD_{67}$-eGFP.

### *In situ* studies using brainstem microinjections

We used an *in situ* decerebrate cardio-pulmonary bypass preparation of mice (Paton, 1995) and rats (Paton & Kasparov, 1999) where partial pressures of circulating gases are clamped, allowing direct recordings of multiple respiratory motor outputs without confounding effects of anaesthesia. Briefly, mice and rats were heparinized (1000 U I.P.) and subsequently anaesthetized deeply with halothane until loss of their paw withdrawal reflex. Mice and rats were decerebrated (precollicular) and the cerebellum was removed to expose IV ventricle and inferior colliculus, then bisected subdiaphragmatically and the head and thorax immersed in ice-cold carbogenated Ringer solution. The left thoracic phrenic (PN) and the left cervical vagus nerve (cVN) were cut distally. In all rats and two mice, the left hypoglossal nerve (XII) was also cut distally. Nerves were recorded using custom made bipolar glass suction electrodes. In the recording chamber, a double lumen catheter (Braintree Scientific, Braintree, MA, USA) was inserted into the descending aorta for retrograde perfusion by a peristaltic roller pump (505Du, Watson Marlow, Falmouth, UK). The perfusion solution consisted of carbogenated (95% $O_2$, 5% $CO_2$ for rats; 94% $O_2$, 6% $CO_2$ for mice) modified Ringer solution at 32°C with an oncotic agent replacing serum albumin (Ficoll, type 70, 1.25%). The second lumen of the catheter was used to monitor aortic perfusion pressure. The baseline perfusate flow was pre-set to 18–20 ml min$^{-1}$ for mice and 21–24 ml min$^{-1}$ for rats. The composition of the Ringer solution was (in mM): NaCl (125); $NaHCO_3$ (24); KCl (3); $CaCl_2$ (2.5); $MgSO_4$ (1.25); $KH_2PO_4$ (1.25); glucose (10); pH 7.35–7.4 after carbogenation. Osmolality was 290 ± 5 mosmol (kg $H_2O$)$^{-1}$. Vecuronium bromide (4 $\mu$g ml$^{-1}$) was added to the perfusion solution to block neuro-muscular transmission and vasopressin (0.5 nM) to increase peripheral vascular resistance, improving brain perfusion. Unless stated, all chemicals were from Sigma-Aldrich. Arterial perfusion pressure was recorded using a Gould transducer and amplifier (Series 6600). Bioelectric signals were amplified (×10,000) and band-pass filtered (0.3–5 kHz) (Differential AC Amplifier Model 1700, A-M Systems, Sequim, WA, USA). Signals were recorded using a CED Micro1401 ADC signal conditioner (10 kHz) and analysed using custom written subroutines in Spike7.10 software (Cambridge Electronic Design, Cambridge, UK).

### Brainstem microinjections

Microinjections were performed using custom made three-barrel glass micropipettes (borosilicate, OD 1.5 mm, ID 0.86 mm, Harvard Apparatus, UK) with 20 $\mu$m outer tip outer diameter. Barrels contained L-glutamate (5–10 mM, Sigma-Aldrich, UK), either bicuculline methochloride (5 mM, Tocris Bioscience, UK) (Bautista & Dutschmann, 2014), or NO-711 hydrochloride (10 $\mu$M, Sigma-Aldrich, UK) or vehicle, and either 2% Evans blue dye (Sigma-Aldrich, UK) or 0.5% red fluorescent microspheres (0.2 $\mu$m, Fluospheres, Life Technologies, F-8763, UK). All drugs were dissolved in artificial cerebrospinal fluid (aCSF) and adjusted to pH 7.4 if needed. Micropipette tips were placed 0.2–0.4 mm caudal to the left inferior colliculus, 1.7–1.8 mm lateral from the midline and 1–1.5 mm ventral to the dorsal surface for mice. In rats, micropipette tips were positioned 0.3–0.5 caudal to inferior colliculus, 1.9–2.1 mm from the midline and 1–1.5 mm of the dorsal surface. Injection volumes were controlled using an ocular reticle in the eyepiece of a surgical microscope. At the beginning of experiments, the depth of injection was functionally identified using glutamate microinjections (30 nL), which elicited an apnoea and prolonged post-inspiratory activity in the cVN when centred in the KF as demonstrated before (Chamberlin & Saper, 1994; Dutschmann & Herbert, 1998, 2006). Microinjection sites were marked after experiments and verified histologically *post hoc*. Brainstems were fixed in 4% paraformaldehyde, cryoprotected in 30% sucrose overnight and sectioned in a freezing microtome (40 $\mu$m). Sections marked with red Fluorospheres were mounted with Vectashield DAPI (VectorLabs, UK). Sections marked with 2% Evans blue dye were Nissl counterstained (2% Neutral Red) and mounted with DPX (Sigma-Aldrich, UK). Microinjection sites were photographed and documented on schematic outlines of the dorsolateral pons (Franklin & Paxinos, 2007).

### Immuno-histochemistry

*Mecp2*$^{+/-}$/GAD$_{67}$-eGFP females ($n = 2$) and *Mecp2*$^{+/+}$/GAD$_{67}$-eGFP littermates ($n = 2$) were killed with pentobarbital (60 mg kg$^{-1}$) and transcardially perfused with 15–20 ml of 4% paraformaldehyde in phosphate buffer (0.1 M, pH 7.4). Their brainstems were cryoprotected overnight in 30% sucrose in phosphate-buffered saline (PBS) at 4°C. Coronal sections (20 $\mu$m) were taken from the pons on a cryostat (Model OTF, Bright Instrument Company, Huntingdon, UK). Once dried onto slides, brain sections were re-hydrated in PBS containing 0.1% Triton (PBST) and blocked in 10% normal goat serum (NGS) in PBST for 30 min at room temperature. Sections were then incubated overnight at 4°C in 10% NGS in PBST containing a polyclonal anti-Mecp2 primary antibody (1:500; raised in rabbit, a generous gift from G. Mandel, Oregon Health & Science University). Sections were washed and incubated with AlexaFluor-647 conjugated goat anti-rabbit IgG (1:500; A-21244, Life Technologies, Paisley, UK) for 1 h at room temperature. The sections were then incubated for 20 min at room temperature with NeuroTrace 530/615 red fluorescent Nissl stain (1:100 in PBS; N-21482, Life Technologies) before being mounted in ProLong Gold (P36934, Life Technologies).

### Image acquisition and analysis

*Mecp2*$^{+/-}$/GAD$_{67}$-eGFP and *Mecp2*$^{+/+}$/GAD$_{67}$-eGFP littermates were processed and imaged in pairs, and every care was taken to maintain the same conditions during fixation, immunolabelling, acquisition and analysis. The KF-nu was identified using anatomical landmarks (Franklin & Paxinos, 2007). Images of the KF nucleus were obtained by confocal laser scanning microscopy using a Leica TCS SP2 AOBS confocal system attached to a Leica DM IRE2 microscope and equipped with argon (488 nm), green HeNe (543 nm), orange HeNe (594 nm), red HeNe (633 nm) and 405 nm lasers (Leica Microsystems, Mannheim). Emission bands were set to 502–554, 572–647 and 652–797 nm, and sequential capture was used to prevent crosstalk. A 100× oil-immersion objective lens (NA 1.4) was used and imaging parameters selected to optimize confocal resolution. Every care was taken to prevent saturated pixels in the field of view. Z-stacks covering a depth of 20 $\mu$m were collected from two tridimensional fields of view (FOV) per left and right hand KF (4 FOVs per section) in a minimum of two sections per mouse. Scans from each channel were taken sequentially and subsequently merged. Images were acquired using the same acquisition parameters for each pair of wild-type and heterozygous mice. Blinded analysis was not possible due to the obvious mosaicism of MECP2 immuno-reactivity (MECP2ir) in HET mice as previously described (Braunschweig *et al.* 2004). To avoid unintentional bias an automated analysis protocol was created with Volocity 3D image analysis software (Perkin Elmer) and applied to all the subjects. GFP-expressing GABAergic perisomatic bouton-like structures were automatically detected as punctate elements within 2 $\mu$m of the 3D outline of red fluorescent Nissl stained perikarya, as previously described by Chattopadhyaya *et al.* (2004). Only perisomatic GFP-expressing structures smaller than 0.5 $\mu$m$^3$ were counted as bouton-like puncta. Likewise, only cells with MECP2 labelled nuclei larger than 10 $\mu$m$^3$, and/or Nissl stained perikarya larger than 250 $\mu$m$^3$ were included in the analysis. These cut-off parameters were estimated by measurements of visually identified structures. Bouton counts are expressed as the number of bouton-like puncta per cell normalized to the wild-type density within the pair of mice. Density of GFP-expressing GABAergic axonal projections are also normalized to the wild-type in the pair.

### Statistical analysis

For comparison of GAD$_{67}$-expressing bouton-like puncta counts we used the Kruskal–Wallis test, followed by Dunn's multiple comparison, and data are reported as median ± interquartile range. For comparing volumes of GAD$_{67}$-expressing processes we used the Mann–Whitney test, and data are reported as median ± interquartile range. Apnoeas were defined as pauses in inspiration that resulted in an expiratory time ($T_E$) 1.5-fold greater than local average $T_E$ in that animal and are expressed as number of apnoeas per hour. In each experiment, 100 respiratory cycles were averaged. For coefficient of variation analysis, apnoeas and periodic breathing were excluded. For comparisons of respiratory parameters which fit a Gaussian distribution (D'Agostino–Pearson omnibus normality test) (Johnson *et al.* 2015), we used one-way ANOVA, followed by Newman–Keuls all pairwise comparison or Dunnett's pairwise comparison *versus* control, where appropriate as stated in figure legends. Parametric data are reported as the mean ± SEM. Prism 6.05 was used for all statistical analysis (GraphPad Software, San Diego, CA, USA). All analysis were performed in the entire sample, without removing outliers. The significance level was set at $P < 0.05$.

## Results

### MECP2 deficient females show reduced perisomatic GABAergic innervation in the KF nucleus

Earlier reports showed defects in GABAergic transmission in the brainstem of RTT mouse models (Medrihan *et al.* 2008), and we have found an excess of post-inspiratory motor drive to the larynx during apnoeas (Abdala *et al.* 2010). Since the KF is an important site for

control of post-inspiratory activity, we sought to compare the number of GABA expressing processes and perisomatic bouton-like puncta on KF nucleus neurones of *Mecp2*$^{+/+}$ ($n = 2$) and *Mecp2*$^{+/-}$ ($n = 2$) double transgenic mice expressing eGFP under the control of the $GAD_{67}$ promoter. We labelled MECP2 immunoreactive (MECP2ir) cells in order to compare cell-autonomous effects of protein deletion. When comparing the percentage of MECP2ir positive and negative cells per FOV in *Mecp2*$^{+/-}$/$GAD_{67}$-eGFP females, we found that $53 \pm 4\%$ of soma were MECP2ir negative ($n = 23$ FOV, 758 soma counted), confirming the previously described mosaicism (Braunschweig *et al.* 2004). In *Mecp2*$^{+/+}$/$GAD_{67}$-eGFP mice, we observed dense GFP-expressing GABAergic innervation to the KF nucleus, but local GABAergic interneurones were very rare and we typically encountered one or no soma per field of view (FOV, $4.5 \times 10^5$ $\mu m^3$) (Fig. 1*C* and *D*). In *Mecp2*$^{+/+}$/$GAD_{67}$-eGFP we analysed 158 soma, and in *Mecp2*$^{+/-}$/$GAD_{67}$-eGFP females we analysed 334 MECP2ir positive and 424 MECP2ir negative soma. Due to the very high density of eGFP expressing processes in *Mecp2*$^{+/+}$ KF nucleus, the number of cells suitable for analysis (i.e. suitably separated from large eGFP processes) was smaller, and hence the difference in number of cells analysed to *Mecp2*$^{+/-}$. The numbers of eGFP-expressing GABAergic bouton-like puncta upon MECP2ir soma of *Mecp2*$^{+/-}$ females was lower than in *Mecp2*$^{+/+}$ littermate females ($2 \pm 8$ *vs.* $37 \pm 51$ boutons/soma, respectively, $P < 0.001$) (Fig. 1*A*). The numbers of eGFP-expressing GABAergic bouton-like puncta upon MECP2ir negative soma ($0 \pm 3$ boutons/soma, $P < 0.001$) was significantly lower compared with either *Mecp2*$^{+/+}$ or MECP2ir-positive soma from *Mecp2*$^{+/-}$ mice (Fig. 1*A*). The total volume per FOV of eGFP-expressing processes was also lower in *Mecp2*$^{+/-}$ females than in *Mecp2*$^{+/+}$ littermates ($0.46 \times 10^3 \pm 1.17 \times 10^3$ *versus* $4.07 \times 10^3 \pm 4.29 \times 10^4$ $\mu m^3$, respectively, $P < 0.001$) (Fig. 1*B*–*D*). Figure 1*Ea* and

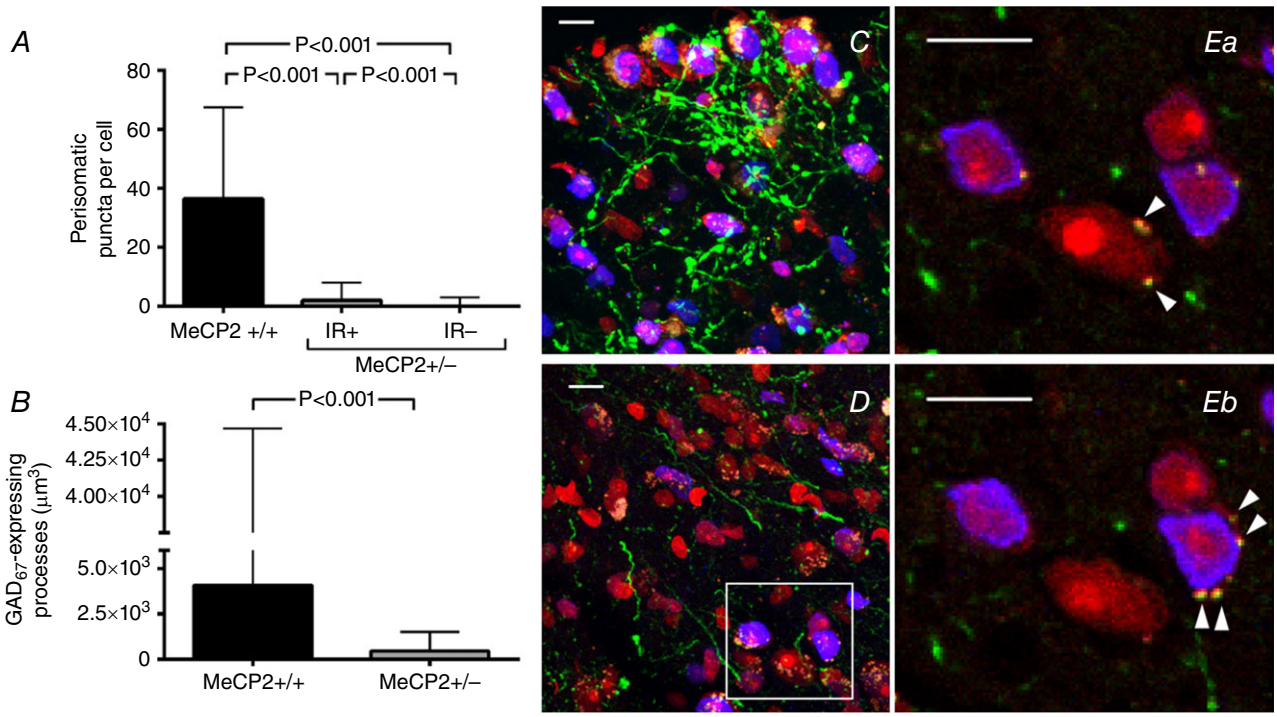


**Figure 1. GABAergic projections in the Kölliker–Fuse nucleus (KF-nu) of *Mecp2*$^{+/-}$/$GAD_{67}$-eGFP compared with the same region in *Mecp2*$^{+/+}$/$GAD_{67}$-eGFP littermate female mice**
GABAergic neurones express eGFP under the control of the $GAD_{67}$ promoter via a knock-in transgene (green); perikarya are labelled in red (Nissl stain) and MECP2 protein immuno-reactive (MECP2ir) nuclei are pseudo-coloured in blue. This $GAD_{67}$-eGFP knock-in strain identifies only parvalbumin GABA processes (Chattopadhyaya *et al.* 2004). *A*, quantification of the number of GABAergic bouton-like puncta per MECP2ir positive (IR+) and negative (IR–) perikarya in the KF of *Mecp2*$^{+/-}$/$GAD_{67}$-eGFP *versus* *Mecp2*$^{+/+}$/$GAD_{67}$-eGFP littermate. *B*, quantification of the volume of GABAergic processes per field of view ($4.5 \times 10^5$ $\mu m^3$). *C* and *D*, representative projection of a z-stack across the KF-nu in a *Mecp2*$^{+/+}$/$GAD_{67}$-eGFP female (*C*) and in a *Mecp2*$^{+/-}$/$GAD_{67}$-eGFP littermate female (*D*). Reduction in MECP2ir is expected in *Mecp2*$^{+/-}$ mice. Note the marked reduction in GFP-expressing GABAergic projections in MECP2 deficient females. *Ea* and *b*, two sequential images of a single confocal plane of the region of interest outlined in *D* showing eGFP-expressing perisomatic puncta (arrowheads) on IR+ and IR– cells. Plots show median ± interquartile range, Kruskal–Wallis test followed by Dunn's multiple comparison test (*A*) and Mann–Whitney test (*B*). Scale bars = 10 $\mu$m.

*b* shows a higher magnification example of GPF-expressing perisomatic puncta in two sequential single confocal plane images in a *Mecp2*$^{+/-}$ female.

### Blockade of GABA reuptake in the KF rescues breathing irregularity in MECP2 deficient females

We hypothesized that the mechanism for generation of respiratory irregularities in MECP2 deficient females involves loss of GABA innervation of the KF. Thus, augmenting endogenous GABA transmission in this area would rescue the respiratory phenotype. To test this, we microinjected NO-711 (10 $\mu$M, 60 nL), a GABA reuptake blocker, directly into the left KF of *Mecp2*$^{+/-}$ females (ipsilateral to nerve recordings). As previously published (Abdala *et al.* 2010), the respiratory phenotype of *Mecp2*$^{+/-}$ females was characterized by recurrent apnoeas and inter-breath irregularity (Fig. 2*A*); blockade of GABA reuptake in the KF ameliorated this phenotype (Fig. 2*B*). All seven *Mecp2*$^{+/-}$ heterozygous females presented a resting number of apnoeas above the upper 95% confidence interval of wild-type mean (41 apnoeas h$^{-1}$). Unilateral microinjections in the KF reduced the occurrence of apnoeas in *Mecp2*$^{+/-}$ females from 204 ± 58 to 70 ± 11 apnoeas h$^{-1}$ ($P < 0.01$, $n = 7$) (Fig. 2*D*), which did not differ significantly from naïve WT littermates (29 ± 5 apnoeas h$^{-1}$, $n = 10$). The coefficient of variation (CV) of expiratory time ($T_E$) was also rescued (0.73 ± 0.09 to 0.37 ± 0.09; $P < 0.01$), equivalent to WT values 0.29 ± 0.06 (Fig. 2*E*). Since $T_E$ is strongly correlated with duration of post-I in the cVN, we also observed reduction in the CV of post-I *Mecp2*$^{+/-}$ females from 0.76 ± 0.07 s to 0.39 ± 0.04 s ($P < 0.001$), comparable to WT levels 0.38 ± 0.05 (Fig. 2*F*). Inspiratory time ($T_I$) was shorter in WT compared with *Mecp2*$^{+/-}$ (0.22 ± 0.03 s *vs.* 0.35 ± 0.03 s) but was not affected by NO-711 treatment in *Mecp2*$^{+/-}$ females (0.38 ± 0.05 s). The following parameters did not differ between WT and *Mecp2*$^{+/-}$ females, and were not affected by NO-711 microinjection in *Mecp2*$^{+/-}$ females: CV of $T_I$ (WT: 0.12 ± 0.03; *Mecp2*$^{+/-}$: 0.19 ± 0.04 pre *vs.* 0.16 ± 0.03 post-NO-711; $P = 0.209$), $T_E$ (WT: 0.93 ± 0.25 s; *Mecp2*$^{+/-}$: 1.0 ± 0.28 s pre *vs.* 0.71 ± 0.1 s post; $P = 0.721$), total respiratory period ($T_{TOT}$) (WT: 1.16 ± 0.27 s; *Mecp2*$^{+/-}$:1.36 ± 0.29 s pre *vs.* 1.09 ± 0.15 s post; $P = 0.785$), PN duty cycle (WT: 27 ± 5%; *Mecp2*$^{+/-}$: 30 ± 5% pre *vs.* 35 ± 2.27% post; $P = 0.356$), and duration of post-I in the cVN (WT: 0.64 ± 0.25 s; *Mecp2*$^{+/-}$: 0.83 ± 0.23 s pre *vs.* 0.51 ± 0.1 s post; $P = 0.620$). The effect of NO-711 microinjections washed out very quickly within 2–3 min, and therefore bilateral injections were not achievable before the effect started wearing off on the first injection site. In some mice NO-711 was microinjected on the right KF after recovery from left side injection, and this had a similar effect on the respiratory phenotype. Vehicle (aCSF) microinjection into the KF at the beginning or at the end of experiments had no effect on respiratory phenotype. Only injection sites centred in the KF, or in close proximity to it, effectively rescued the respiratory phenotype (Fig. 2*C*). Figure 4*A* and *B* shows an example histological image of a mouse dorsolateral pons with a microinjection site marked with dye at the end of the experiment.

### Blockade of $GABA_A$ receptors in the KF recapitulates respiratory phenotype from RTT

We postulated that if loss of GABA synaptic transmission in the KF is sufficient for generation of respiratory irregularities in *Mecp2*$^{+/-}$ females, then mimicking this deficiency by blocking $GABA_A$ receptors in the KF of WT rats should generate a Rett-like respiratory phenotype. To test this, we microinjected bicuculline (5 mM, 60 nL), a $GABA_A$ receptor antagonist, bilaterally into the KF of Wistar rats. Microinjections were performed first on the left KF and within 1 min on the right side, after functional identification with glutamate. Respiratory parameters were evaluated before, and after unilateral (UNI) and bilateral (BI) microinjections. Wistar rats were used as they presented a very regular respiratory pattern with no spontaneous central apnoeas (Fig. 3*A*); contrary C57BL6/J mice display breathing irregularities and apnoeas (Stettner *et al.* 2008*a*,*b*). Hence, rats were chosen for this protocol instead of mice. Blockade of $GABA_A$ synaptic transmission in the KF induced recurrent PN apnoeas after bilateral blockade in 8/8 rats (256 ± 27 apnoeas h$^{-1}$; $P < 0.01$) (Fig. 3*A* and *B*). After unilateral microinjection only 4/8 rats developed apnoeas (32 ± 16 apnoeas h$^{-1}$, $P > 0.05$) and of these, only two rats presented more than 50 apnoeas h$^{-1}$ (Fig. 3*B*). The average length of apnoeas did not differ significantly between unilateral and bilateral blockade (UNI: 2.61 ± 1.07 s, BI: 3.94 ± 0.62 s). The effects of bicuculline dissipated 40–60 min after the microinjections and central apnoeas ceased. Similarly to *Mecp2*$^{+/-}$ mice, $GABA_A$ blockade in the KF of rats induced rhythm irregularity and increased the coefficient of variation of $T_E$ (control: 0.1 ± 0.01; UNI: 0.25 ± 0.05, $P < 0.05$; BI: 0.67 ± 0.06, $P < 0.01$) (Fig. 3*C*). The CV of $T_I$ was also increased significantly (control: 0.04 ± 0.01; UNI: 0.13 ± 0.02, $P > 0.05$; BI: 0.31 ± 0.04, $P < 0.01$). Similarly to *Mecp2*$^{+/-}$ mice, $T_E$ is strongly correlated with duration of post-I in the cVN, and we also saw an increase in the CV of post-I after bilateral $GABA_A$ blockade (control: 0.15 ± 0.02; UNI: 0.28 ± 0.05, $P > 0.05$; BI: 0.68 ± 0.06, $P < 0.01$) (Fig. 3*D*). The mean duration of post-I in the cVN nerve decreased only after bilateral injections (control: 2.2 ± 0.4 s; UNI: 1.8 ± 0.2 s, $P > 0.05$; BI: 1.6 ± 0.2 s, $P < 0.05$). $T_{TOT}$ was reduced by microinjections (control: 3.8 ± 0.4 s; UNI: 2.9 ± 0.2 s, $P < 0.01$; BI: 2.8 ± 0.2 s, $P < 0.01$), which was entirely due to a reduction in $T_E$ (control: 3.1 ± 0.4 s; UNI: 2.2 ± 0.2 s,

$P < 0.05$; BI: 1.9 ± 0.2 s, $P < 0.01$), with $T_I$ remaining unchanged (control: 0.75 ± 0.04 s; UNI: 0.67 ± 0.08 s; BI: 0.81 ± 0.08 s). PN duty cycle increased after bilateral blockade of $GABA_A$ receptors (control: 21 ± 2%; UNI: 23 ± 3%, $P > 0.05$; BI: 30 ± 3%, $P < 0.01$). Microinjections did not change mean PN amplitude ($P = 0.343$), cVN burst envelope during inspiration ($P = 0.150$) and expiration ($P = 0.401$), cVN post-I peak ($P = 0.236$), and cVN pre-inspiratory nadir ($P = 0.143$). Only injection sites centred in the KF, or in close proximity to it, effectively reproduced a Rett-like respiratory phenotype (Fig. 3*E*). In some rats, bicuculline microinjections were repeated after the washout period and produced a similar effect. Vehicle (aCSF) microinjection into the KF at the

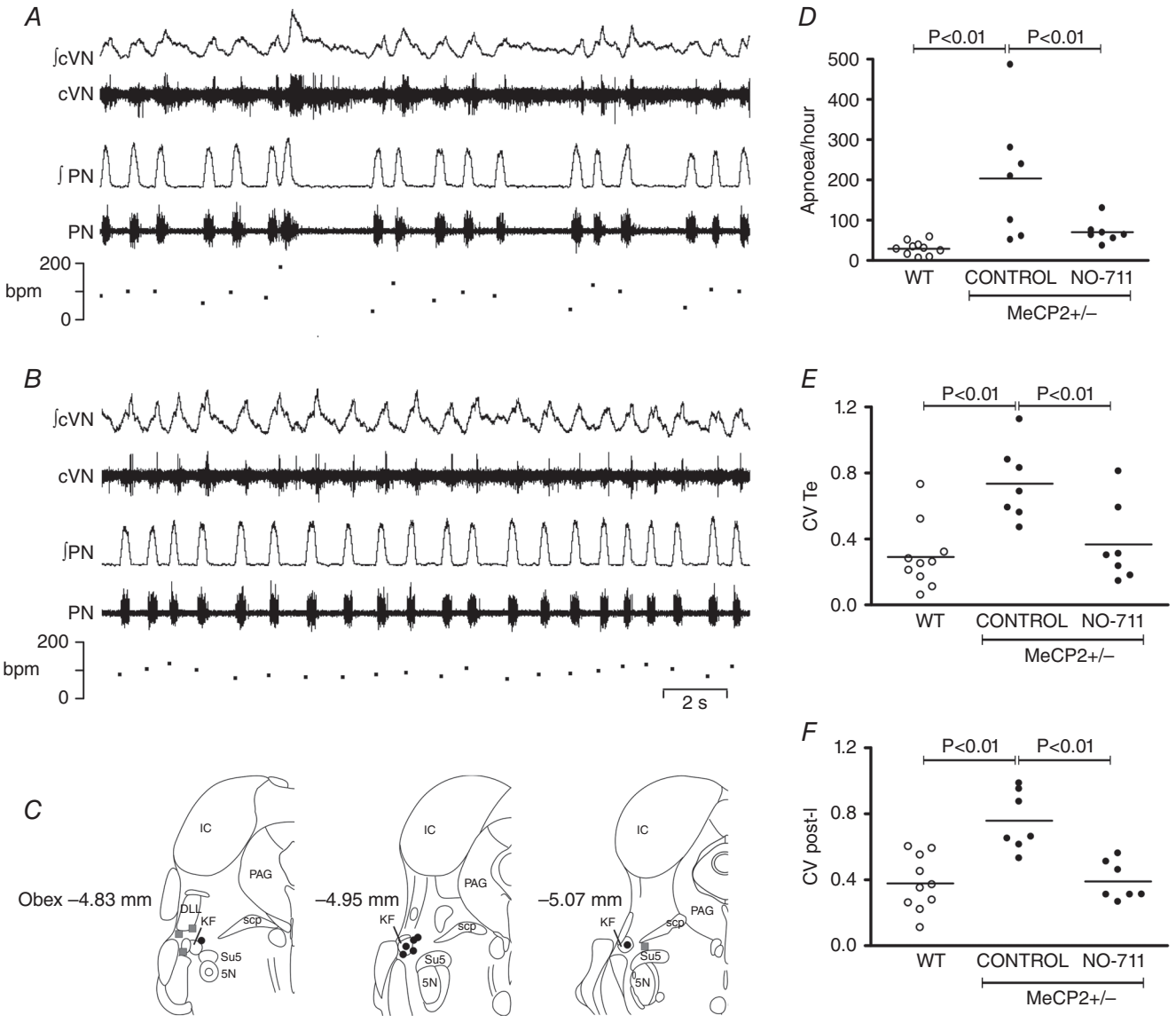


**Figure 2. Blockade of GABA reuptake in the Kölliker–Fuse area (KF) rescued respiratory phenotype of MECP2 deficient females (*Mecp2*$^{+/-}$, $n = 7$) to wild-type (WT, $n = 10$) levels**
*A*, typical trace showing resting phrenic nerve (PN), central vagus nerve (cVN) and respiratory rate in a *Mecp2*$^{+/-}$ female mouse. *B*, the same *Mecp2*$^{+/-}$ mouse after microinjection of NO-711 (GABA reuptake blocker, 10 $\mu$M, 60 nL) in the KF. *C*, schematic diagram modified from (Franklin & Paxinos, 2007) showing effective (black circles) and non-effective (grey squares) microinjection sites (section distances from obex). Abbreviations: 5 N, motor trigeminal nucleus; DLL, dorsal nucleus of the lateral lemniscus; IC, inferior colliculus; PAG, periaqueductal grey; scp, superior cerebellar peduncle; Su5, supratrigeminal nucleus. *D*, blockade of GABA reuptake in the KF reduced occurrence of apnoeas in *Mecp2*$^{+/-}$ female mice (filled circles, $n = 7$) to the level of littermate wild-type females (open circles, $n = 10$). *E*, microinjections also reduced the coefficient of variation (CV) of expiratory time ($T_E$) in the PN, and the CV of post-inspiration (post-I) in the cVN to that of WT females (*F*). Plots show individual values (circles) and means (lines), one-way ANOVA, Newman–Keuls all pairwise comparison.

beginning or at the end of experiments had no effect on breathing. Figure 4*C* and *D* shows an example histological image of a rat dorsolateral pons with a microinjection site marked with dye at the end of the experiment.

Some of the respiratory motor output effects of bilateral blockade of $GABA_A$ receptors in the KF of healthy rats recapitulated those seen in *Mecp2*$^{+/-}$ mice. Periods of apnoea were typically characterized by abnormal XII activity during exhalation (Fig. 5*Aa* and *b*) followed by weakened/absent inspiratory coupling on the ensuing breath, and exaggerated post-inspiratory output in the cVN (Fig. 5*Ba* and *b*). Most remarkable, was the periodic breathing pattern (Fig. 3*A*), which is characterized by periods of apnoea intercalated with hypopnea and hyperventilation, and is often present in RTT (Julu *et al.* 2001; Abdala *et al.* 2010). This is translated into a characteristic distribution pattern in the Poincaré plots with clusters of very high and very low frequency breaths that typically lay outside normal breathing frequency range (Fig. 5*Ca* and *b*).

## Discussion

In the present study we demonstrated a dramatic reduction in the number of local KF GABAergic processes and perisomatic bouton-like puncta on all perikarya of *Mecp2*$^{+/-}$/$GAD_{67}$-eGFP mice compared with *Mecp2*$^{+/+}$/$GAD_{67}$-eGFP mice. In *Mecp2*$^{+/-}$ KF, the loss of GABAergic puncta was more pronounced in mutant cells than in wild-type. Additionally, we found that the respiratory phenotype of *Mecp2*$^{+/-}$ mice was rescued by microinjections of a GABA reuptake blocker

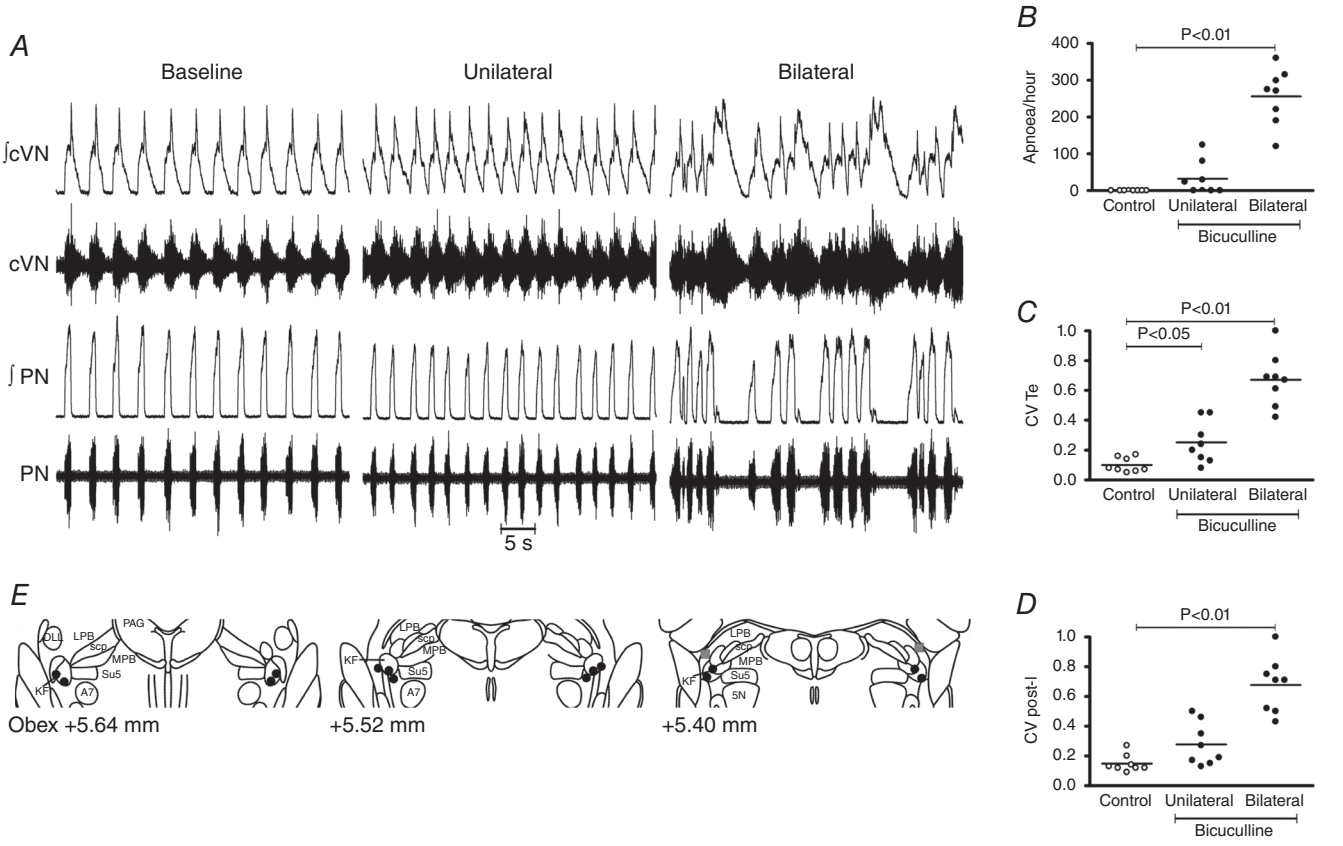


**Figure 3. Blockade of $GABA_A$ receptors in the Kölliker–Fuse area (KF) induced Rett-like respiratory phenotype in wild-type rats ($n = 8$)**
*A*, typical trace showing phrenic nerve (PN), central vagus nerve (cVN) during a control period and after unilateral and bilateral microinjection of bicuculline (5 mM, 60 nL), a $GABA_A$ receptor antagonist. *B*, central apnoeas were absent in wild-type rats (open circles), and unilateral and bilateral blockade of $GABA_A$ receptors induced central apnoeas in 4/8 and 8/8 rats, respectively (filled circles). *C* and *D*, microinjections also increased the coefficient of variation of expiratory time ($T_E$) in the PN (*C*), and the coefficient of variation of post-inspiration (post-I) (*D*). *E*, schematic diagram modified from Franklin and Paxinos (2007) showing effective (black circles) and non-effective (grey squares) bilateral microinjection sites. Abbreviations: 5 N, motor trigeminal nucleus; A7, facial motor nucleus; DLL, dorsal nucleus of the lateral lemniscus; MPB, medial parabrachial nucleus; LPB, lateral parabrachial nucleus; PAG, periaqueductal grey; scp, superior cerebellar peduncle; Su5, supratrigeminal nucleus. Plots show individual values (circles) and means (lines), one-way ANOVA, Dunnett's pairwise comparison *versus* control.

in the KF parenchyma, to increase the availability of endogenous GABA in this area. Moreover, the respiratory phenotype observed in *Mecp2*$^{+/-}$ was recapitulated by microinjections of a $GABA_A$ receptor antagonist into KF parenchyma of healthy wild-type rats, to disrupt local GABA synaptic transmission in this area. One limitation of microinjection techniques is that we cannot rule out spread of the drugs to neighbouring regions in the parabrachial complex. However, the lateral and medial parabrachial nuclei have ascending projections to targets in the forebrain, while only a small population of the lateral parabrachial nuclei (lateral crescent) have descending brainstem projections and the medial parabrachial in rats is largely gustatory (Dutschmann & Dick, 2012). Within the parabrachial complex only the KF has strong descending connectivity with respiratory nuclei in pons and medulla (Dutschmann & Dick, 2012). Consequently, microinjections outside the KF were less effective. The effects of blocking GABAergic synaptic transmission in the KF were studied by others *in situ* (Bautista & Dutschmann, 2014), and *in vivo* (Dutschmann & Herbert, 1998; Damasceno *et al.* 2014), and although rhythm irregularity was mentioned, pattern changes had not been described in detail. In the present study, we described a pattern of periodic breathing after KF disinhibition reminiscent of *Mecp2*$^{+/-}$ respiratory phenotype. The positive effects after local (here) or systemic (Abdala *et al.* 2010) treatment with GABA reuptake blockers in MECP2 deficient mice, may seem counterintuitive given the extreme paucity of GABAergic boutons observed in *Mecp2*$^{+/-}$ females in the present study. However, it is likely that this study underestimated the numbers of GABA releasing projections in the KF because the $GAD_{67}$-eGFP transgene identifies parvalbumin GABA processes but does not label somatostatin or cholecystokinin GABA subtypes (Chattopadhyaya *et al.* 2004). Despite those limitations, our data suggest that deficits of GABAergic synaptic inhibition in the KF contribute to respiratory dysrhythmia in this rodent model of RTT.

Early single-photon emission computed tomography studies in human patients with RTT detected reduced benzodiazepine receptor binding in their brains,

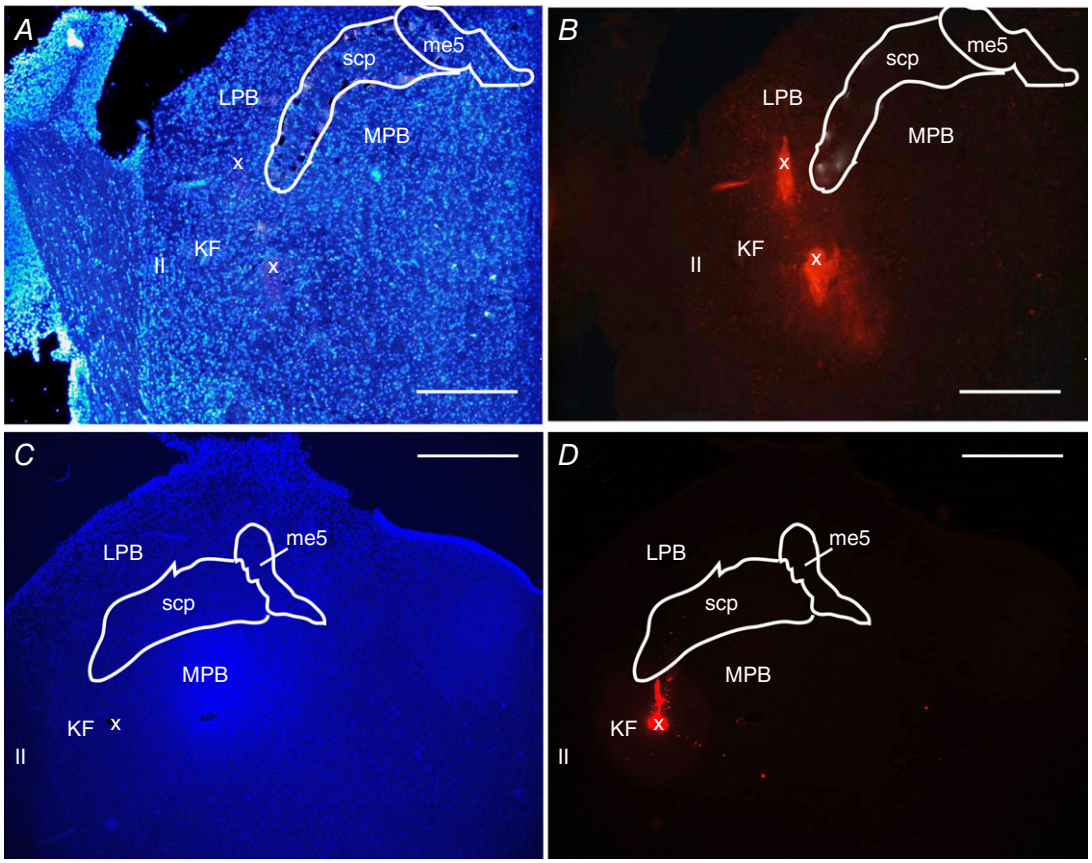


**Figure 4. Example histological photomicrographs of microinjection sites in the Kölliker–Fuse area (KF)**
*A* and *B*, dorsolateral pons of a *Mecp2*$^{+/-}$ female mouse counterstained with DAPI *(A)* showing microinjection site labelled with red fluorescent beads (x) (*B*). *C* and *D*, dorsolateral pons of a Wistar rat counterstained with DAPI *(C)* showing microinjection site marked with red fluorescent beads (x) (*D*). Anatomical landmarks: ll, lateral lemniscus; me5, mesencephalic trigeminal nucleus; MPB, medial parabrachial nucleus; LPB, lateral parabrachial nucleus; scp, superior cerebellar peduncle. Scale bars = 500 $\mu$m.

suggesting a deficiency in GABA receptor-mediated synaptic transmission (Yamashita *et al.* 1998). However, post-mortem studies showed that GABA receptor densities were elevated in certain brain areas, e.g. basal ganglia (Blue *et al.* 1999*a*) and superior frontal gyrus (Blue *et al.* 1999*b*). This indicates a possible compensatory mechanism due to reduced pre-synaptic release of GABA. The first evidence that GABAergic neurones might be affected in RTT was the finding that the transcription factor Dlx5 is regulated by MECP2, as it promotes differentiation and maturation of forebrain GABAergic neurones (Horike *et al.* 2005). In *Mecp2* null males, Medrihan *et al.* (2008) demonstrated a decrease in GABAergic but not glycinergic transmission in the ventrolateral medullary respiratory network. The loss of KF GABAergic innervation that we observed in *Mecp2*$^{+/-}$ mice may involve contribution of mutant glia in a non-cell-autonomous manner. *Mecp2* is expressed in astroglia (Yasui *et al.* 2013; Forbes-Lorman *et al.* 2014), and loss of MECP2 impairs astrocytic glutamate clearance (Okabe *et al.* 2012) promoting dendritic damage in neurones (Ballas *et al.* 2009; Maezawa & Jin, 2010). In the present study, we observed that loss of GABAergic terminal projections depended on local non-cell-autonomous and cell-autonomous mechanisms,

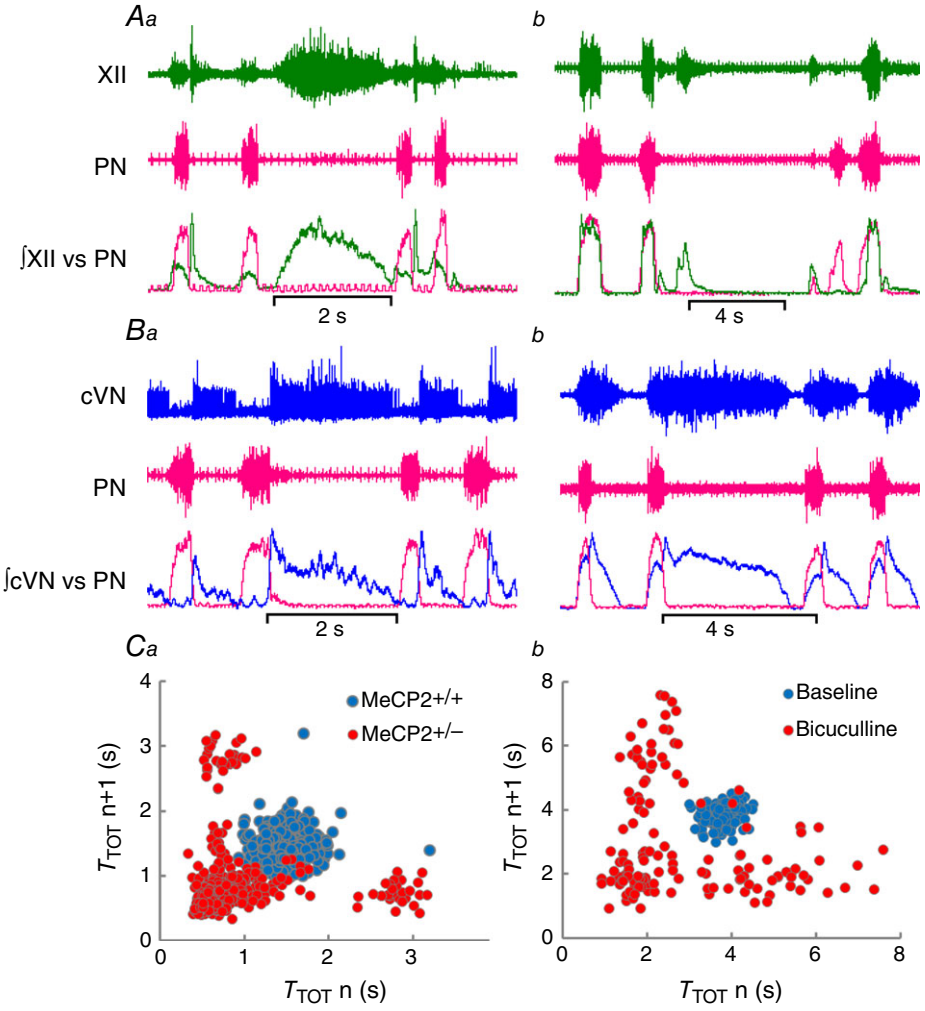


**Figure 5. Comparison of respiratory motor outputs in *Mecp2*$^{+/-}$ mice versus effects of blocking Kölliker–Fuse area (KF) GABA$_A$ receptors in wild-type (WT) rats**
*A*, typical traces of the hypoglossal (XII) and phrenic (PN) nerve activities during an apnoea in a *Mecp2*$^{+/-}$ mouse (*Aa*) and after bilateral blockade of KF GABA$_A$ receptors (bicuculline, 5 mM, 60 nL) in a WT rat (*Ab*). Note XII activity during apnoea, and temporary loss inspiratory drive in the first breath after apnoea. *B*, typical traces of the cervical vagus (cVN) and phrenic (PN) nerve activities during an apnoea in a *Mecp2*$^{+/-}$ mouse (*Ba*) and after bilateral blockade of KF GABA$_A$ receptors in a WT rat (*Bb*). Note post-inspiratory activity in the cVN throughout the apnoeas. *C*, Poincaré plots of total respiratory period ($T_{TOT}$) in a *Mecp2*$^{+/-}$ mouse (*Ca*) presenting periodic breathing, and after bilateral blockade of KF GABA$_A$ receptors in a WT rat (*Cb*). Note similar scattering of PN period in *Mecp2*$^{+/-}$ and in bicuculline induced breathing dysrhythmia in rats, typical of periodic breathing.

with the latter contributing to a lesser degree. This indicates a role for mutant glia on the KF inhibitory circuitry damage in this mouse model of RTT. Loss of MECP2 on inhibitory neurones themselves also contributes to the pathology of RTT. Mice lacking MECP2 in neurones expressing the vesicular inhibitory amino-acid transporter (VIAAT) (Chao *et al.* 2010) recapitulated many of the motor-behavioural deficits of RTT, including recurrent apnoeas and irregular rhythm. In line with those findings, we had first demonstrated that GABA mimetic drugs rescued the respiratory abnormalities in both null males and *Mecp2*$^{+/-}$ female mice (Abdala *et al.* 2010), which was later confirmed by others (Voituron & Hilaire, 2011). Consistent with the murine data, case studies also reported a positive effect of GABA mimetics on breathing in patients with RTT (Goyal *et al.* 2004; Krajnc, 2014). Our present findings confirm that GABAergic transmission deficits, presumably caused by MECP2 deficiency, underlie the respiratory dysrhythmia in RTT, and highlights deficits of pre-synaptic mechanisms in the KF as a potential major contributor.

The KF, a constituent of the pneumotaxic centre (Gautier & Bertrand, 1975), controls inspiratory–expiratory phase transition, and in particular expiratory airflow patterns (Dutschmann & Herbert, 2006). In addition to autonomic control, it also integrates respiratory adaptation to behaviours like vocalization and swallowing (Dutschmann & Dick, 2012). Stimulation of this area off-switches inspiration and lengthens expiration to the extreme of producing an apnoea (Cohen, 1971; Chamberlin & Saper, 1994). Dutschmann & Herbert (2006) showed those apnoeas were characterized by expiratory overactivity of the recurrent laryngeal branch of the vagus nerve resulting in activation of glottal adductor muscles throughout the apnoea. In a previous study, we demonstrated that typical apnoeas in Rett mice were characterized by overactivity of expiratory motor outputs, in particular the vagal drive to the larynx but also hypoglossal and abdominal motor outputs (Abdala *et al.* 2010). We had also demonstrated that systemic administration, as well as KF microinjections, of a 5-HT$_{1A}$ receptor agonist corrected respiratory irregularities in a mouse model of RTT (Abdala *et al.* 2014*b*). It is plausible that activation of 5-HT$_{1A}$ receptors in the KF and possibly in downstream post-inspiratory neurones located in the Bötzinger complex (systemic administration) (Richter *et al.* 2003) hyperpolarized them, rescuing the expiratory overactivity and the rhythm irregularity (for review see (Abdala *et al.* 2014*a*). In line with previous data, we have presently confirmed an important role for the KF in the generation of apnoeas in RTT and demonstrate a critical defect on GABA synaptic drives to this region as a contributing factor.

The interconnections between left and right KF (Song *et al.* 2012) may also explain why the RTT-like respiratory arrhythmias were only fully evident after bilateral (as opposed to unilateral) instillations of bicuculline. The fact that unilateral facilitation of GABAergic transmission was sufficient to rescue the respiratory phenotype in RTT suggests that inhibitory circuitry in one KF is sufficient to prevent rhythm irregularity. This may not be entirely surprising since in addition to the multiple innervations to its contralateral counterpart, the KF also has ipsi- and contralateral projections to parabrachial complex nuclei and nucleus tractus solitarii (NTS) (Song *et al.* 2012). In this context, the respiratory phenotype present in mouse models of MECP2 deficiency has been associated with defects in other neurotransmitter systems and brainstem regions including the NTS (Kline *et al.* 2010; Kron *et al.* 2014) and pre-Bötzinger complex (Viemari *et al.* 2005). Additionally, GABAergic innervation deficits have also been shown in other respiratory nuclei in the brainstem. Medrihan *et al.* (2008) described reduction in VIAAT-immunoreactive puncta in the ventral respiratory column (in a region encompassing pre-Bötzinger and Bötzinger complexes) of *Mecp2* null males. Our data do not exclude a possible contribution of these regions for the complex respiratory phenotypes associated with Rett syndrome, which include abnormalities in central chemoreflex sensitivity and hypoxic ventilatory responses (Bissonnette & Knopp, 2008; Voituron *et al.* 2009; Kron *et al.* 2011; Zhang *et al.* 2011; Toward *et al.* 2013; Bissonnette *et al.* 2014). Nevertheless, the presented data provide functional evidence of a significant contribution of GABA$_A$-ergic circuitry within the KF for the rhythm irregularity and recurrent apnoeas that seem to be crucial for the overall respiratory deficits in RTT.

Here, we demonstrated a dense network of GABAergic bouton-like puncta expressing eGFP under the control of the GAD$_{67}$ promoter in the KF, as opposed to sparsely distributed GFP-expressing soma, which is in line with previously published data (Guthmann *et al.* 1998). This highlights a role for external sources of GABAergic inhibition. Perhaps the most studied source of inhibitory input to KF is the NTS. Anatomical studies have shown GABA projections from NTS to KF neurones that in turn project to the rostral ventral respiratory group and phrenic nucleus (Yokota *et al.* 2008). Electrophysiological methods of antidromic mapping demonstrated projections of NTS pump cells, which are largely GABAergic (Ezure & Tanaka, 2004), to KF neurones (Ezure *et al.*, 1998, 2002). It is logical to infer that deficits of inhibitory synaptic transmission in this NTS–KF axis, which integrates afferent input from lung inflation/deflation, would result in respiratory rhythm instability. Indeed, abnormalities of vagally mediated reflexes have been described in MECP2 deficient mice (Stettner *et al.* 2007;

Song *et al.* 2011; Dhingra *et al.* 2013). However, the respiratory dysrhythmia in *Mecp2*$^{+/-}$ and *Mecp2*$^{-/-}$ mice persisted even after removal of lung stretch receptors in the arterially perfused *in situ* preparation (Abdala *et al.* 2010), suggesting that other sources of synaptic inhibition to the KF may play an equally important role in rhythm stability. Among these are inhibitory augmenting expiratory (E-AUG) neurones from the Bötzinger complex (Ezure *et al.* 2003*b*), which provide extensive phasic inhibition to medullary inspiratory and post-inspiratory neurones during late-expiration and are likely to co-release GABA and glycine (Champagnat *et al.* 1982; Haji *et al.* 1992; Schmid *et al.* 1996; Schreihofer *et al.* 1999; Ezure *et al.* 2003*a*; Fortuna *et al.* 2008). These projections are presumably responsible for the inhibitory postsynaptic potentials demonstrated during the late-expiratory phase in subpopulations of KF neurones (Dick *et al.* 1994). Possible deficits in this inhibitory pathway in *Mecp2*$^{+/-}$ mice make for another likely neural substrate for excessive descending KF drive during post-I. Somatostatin-expressing neurones from the pre-Bötzinger (pre-BötC) complex were also found to project to the KF (Tan *et al.* 2010). However, only a very small portion of somatostatin expressing pre-BötC inspiratory neurones were found to co-express $GAD_{67}$ (Stornetta *et al.* 2003) making them a less likely contributor to KF overexcitability in RTT.

The present study was the first to demonstrate the KF as the candidate locus within the brain responsible for rhythm irregularity in RTT. Additionally, we have identified KF GABAergic synaptic transmission as the main system at fault, and demonstrated its effects on the rhythm, pattern and coordination of multiple respiratory motor outputs. The present results are valuable for informing current treatments because they corroborate the hypothesis that central apnoeas, periodic breathing and upper airway obstruction are a product of the same faulty mechanism particular to RTT, and should not be addressed separately (Ramirez *et al.* 2013). Crucially, Bautista & Dutschmann (2014) reported a pattern of motor activity in the larynx upon KF disinhibition that would be conducive to aspiration during swallowing. These events along with air swallowing are common in patients with RTT and generate difficulties in feeding to the point of requiring gastrostomy (Morton *et al.*, 1997, 2000; Isaacs *et al.* 2003; Downs *et al.* 2014). Our data in mice and rat suggest the possibility that swallowing and respiratory dysfunction in RTT may share a common origin: KF disinhibition. It is also noteworthy that changes in breathing driven by emotional state, such as anxiety, are relayed from suprapontine regions to the medulla via the parabrachial complex, which includes the KF (Hayward *et al.* 2004). Interestingly, Ren *et al.* (2012), demonstrated that at least in null males, in early stages of the disease, stress and anxiety were a significant factor triggering the respiratory phenotype. Our data in mice and rat suggest the possibility that deficits in KF inhibition could also facilitate the relay of abnormal drive from suprapontine regions in RTT. For those reasons we propose that therapies targeted to the KF could successfully rescue the multifactorial respiratory phenotypes in RTT.

## References


Abdala AP, Bissonnette JM & Newman-Tancredi A (2014*a*). Pinpointing brainstem mechanisms responsible for autonomic dysfunction in Rett syndrome: therapeutic perspectives for 5-HT1A agonists. *Front Physiol* **5**, 205.

Abdala AP, Dutschmann M, Bissonnette JM & Paton JF (2010). Correction of respiratory disorders in a mouse model of Rett syndrome. *Proc Natl Acad Sci USA* **107**, 18208–18213.

Abdala AP, Lioy DT, Garg SK, Knopp SJ, Paton JF & Bissonnette JM (2014*b*). Effect of Sarizotan, a 5-HT1a and D2-like receptor agonist, on respiration in three mouse models of Rett syndrome. *Am J Respir Cell Mol Biol* **50**, 1031–1039.

Alheid GF, Gray PA, Jiang MC, Feldman JL & McCrimmon DR (2002). Parvalbumin in respiratory neurons of the ventrolateral medulla of the adult rat. *J Neurocytol* **31**, 693–717.

Ballas N, Lioy DT, Grunseich C & Mandel G (2009). Non-cell autonomous influence of MeCP2-deficient glia on neuronal dendritic morphology. *Nat Neurosci* **12**, 311–317.

Bautista TG & Dutschmann M (2014). Ponto-medullary nuclei involved in the generation of sequential pharyngeal swallowing and concomitant protective laryngeal adduction in situ. *J Physiol* **592**, 2605–2623.

Bissonnette JM & Knopp SJ (2008). Effect of inspired oxygen on periodic breathing in methy-CpG-binding protein 2 (Mecp2) deficient mice. *J Appl Physiol* **104**, 198–204.

Bissonnette JM, Schaevitz LR, Knopp SJ & Zhou Z (2014). Respiratory phenotypes are distinctly affected in mice with common Rett syndrome mutations MeCP2 T158A and R168X. *Neuroscience* **267**, 166–176.

Blue ME, Naidu S & Johnston MV (1999*a*). Altered development of glutamate and GABA receptors in the basal ganglia of girls with Rett syndrome. *Exp Neurol* **156**, 345–352.

Blue ME, Naidu S & Johnston MV (1999*b*). Development of amino acid receptors in frontal cortex from girls with Rett syndrome. *Ann Neurol* **45**, 541–545.

Braunschweig D, Simcox T, Samaco RC & LaSalle JM (2004). X-Chromosome inactivation ratios affect wild-type MeCP2 expression within mosaic Rett syndrome and *Mecp2*$^{-/+}$ mouse brain. *Hum Mol Genet* **13**, 1275–1286.

Carotenuto M, Esposito M, D'Aniello A, Rippa CD, Precenzano F, Pascotto A, Bravaccio C & Elia M (2012). Polysomnographic findings in Rett syndrome: a case-control study. *Sleep Breath* **17**, 93–98.

Chamberlin NL & Saper CB (1994). Topographic organization of respiratory responses to glutamate microstimulation of the parabrachial nucleus in the rat. *J Neurosci* **14**, 6500–6510.

Champagnat J, Denavit-Saubie M, Moyanova S & Rondouin G (1982). Involvement of amino acids in periodic inhibitions of bulbar respiratory neurones. *Brain Res* **237**, 351–365.

Chao HT, Chen H, Samaco RC, Xue M, Chahrour M, Yoo J, Neul JL, Gong S, Lu HC, Heintz N, Ekker M, Rubenstein JL, Noebels JL, Rosenmund C & Zoghbi HY (2010). Dysfunction in GABA signalling mediates autism-like stereotypies and Rett syndrome phenotypes. *Nature* **468**, 263–269.

Chattopadhyaya B, Di Cristo G, Higashiyama H, Knott GW, Kuhlman SJ, Welker E & Huang ZJ (2004). Experience and activity-dependent maturation of perisomatic GABAergic innervation in primary visual cortex during a postnatal critical period. *J Neurosci* **24**, 9598–9611.

Cohen MI (1971). Switching of the respiratory phases and evoked phrenic responses produced by rostral pontine electrical stimulation. *J Physiol* **217**, 133–158.

Damasceno RS, Takakura AC & Moreira TS (2014). Regulation of the chemosensory control of breathing by Kolliker-Fuse neurons. *Am J Physiol Regul Integr Comp Physiol* **307**, R57–67.

Dhingra RR, Zhu Y, Jacono FJ, Katz DM, Galan RF & Dick TE (2013). Decreased Hering-Breuer input-output entrainment in a mouse model of Rett syndrome. *Front Neural Circuits* **7**, 42.

Dick TE, Bellingham MC & Richter DW (1994). Pontine respiratory neurons in anesthetized cats. *Brain Res* **636**, 259–269.

Downs J, Wong K, Ravikumara M, Ellaway C, Elliott EJ, Christodoulou J, Jacoby P & Leonard H (2014). Experience of gastrostomy using a quality care framework: the example of Rett syndrome. *Medicine (Baltimore)* **93**, e328.

Dutschmann M & Dick TE (2012). Pontine mechanisms of respiratory control. *Compr Physiol* **2**, 2443–2469.

Dutschmann M & Herbert H (1998). NMDA and $GABA_A$ receptors in the rat Kolliker-Fuse area control cardiorespiratory responses evoked by trigeminal ethmoidal nerve stimulation. *J Physiol* **510**, 793–804.

Dutschmann M & Herbert H (2006). The Kolliker-Fuse nucleus gates the postinspiratory phase of the respiratory cycle to control inspiratory off-switch and upper airway resistance in rat. *Eur J Neurosci* **24**, 1071–1084.

Ezure K & Tanaka I (2004). GABA, in some cases together with glycine, is used as the inhibitory transmitter by pump cells in the Hering-Breuer reflex pathway of the rat. *Neuroscience* **127**, 409–417.

Ezure K, Tanaka I & Kondo M (2003*a*). Glycine is used as a transmitter by decrementing expiratory neurons of the ventrolateral medulla in the rat. *J Neurosci* **23**, 8941–8948.

Ezure K, Tanaka I & Miyazaki M (1998). Pontine projections of pulmonary slowly adapting receptor relay neurons in the cat. *Neuroreport* **9**, 411–414.

Ezure K, Tanaka I & Saito Y (2003*b*). Brainstem and spinal projections of augmenting expiratory neurons in the rat. *Neurosci Res* **45**, 41–51.

Ezure K, Tanaka I, Saito Y & Otake K (2002). Axonal projections of pulmonary slowly adapting receptor relay neurons in the rat. *J Comp Neurol* **446**, 81–94.

Forbes-Lorman RM, Kurian JR & Auger AP (2014). MeCP2 regulates GFAP expression within the developing brain. *Brain Res* **1543**, 151–158.

Fortuna MG, West GH, Stornetta RL & Guyenet PG (2008). Botzinger expiratory-augmenting neurons and the parafacial respiratory group. *J Neurosci* **28**, 2506–2515.

Franklin KBJ & Paxinos G (2007). *The Mouse Brain in Stereotaxic Coordinates*. Elsevier, Amsterdam.

Gautier H & Bertrand F (1975). Respiratory effects of pneumotaxic center lesions and subsequent vagotomy in chronic cats. *Resp Physiol* **23**, 71–85.

Goyal M, O'Riordan MA & Wiznitzer M (2004). Effect of topiramate on seizures and respiratory dysrhythmia in Rett syndrome. *J Child Neurol* **19**, 588–591.

Guthmann A, Fritschy JM, Ottersen OP, Torp R & Herbert H (1998). GABA, GABA transporters, $GABA_A$ receptor subunits, and GAD mRNAs in the rat parabrachial and Kolliker-Fuse nuclei. *J Comp Neurol* **400**, 229–243.

Haji A, Takeda R & Remmers JE (1992). Evidence that glycine and GABA mediate postsynaptic inhibition of bulbar respiratory neurons in the cat. *J Appl Physiol (1985)* **73**, 2333–2342.

Hayward LF, Castellanos M & Davenport PW (2004). Parabrachial neurons mediate dorsal periaqueductal gray evoked respiratory responses in the rat. *J Appl Physiol (1985)* **96**, 1146–1154.

Horike S, Cai S, Miyano M, Cheng JF & Kohwi-Shigematsu T (2005). Loss of silent-chromatin looping and impaired imprinting of DLX5 in Rett syndrome. *Nat Genet* **37**,31–40.

Isaacs JS, Murdock M, Lane J & Percy AK (2003). Eating difficulties in girls with Rett syndrome compared with other developmental disabilities. *J Am Diet Assoc* **103**, 224–230.

Johnson CM, Cui N, Zhong W, Oginsky MF & Jiang C (2015). Breathing abnormalities in a female mouse model of Rett syndrome. *J Physiol Sci* **65**, 451–459.

Julu PO, Kerr AM, Apartopoulos F, Al-Rawas S, Engerstrom IW, Engerstrom L, Jamal GA & Hansen S (2001). Characterisation of breathing and associated central autonomic dysfunction in the Rett disorder. *Arch Dis Child* **85**, 29–37.

Kline DD, Ogier M, Kunze DL & Katz DM (2010). Exogenous brain-derived neurotrophic factor rescues synaptic dysfunction in Mecp2-null mice. *J Neurosci* **30**, 5303–5310.

Krajnc N (2014). Severe respiratory dysrhythmia in Rett syndrome treated with topiramate. *J Child Neurol* **29**, NP118–121.

Kron M, Lang M, Adams IT, Sceniak M, Longo F & Katz DM (2014). A BDNF loop-domain mimetic acutely reverses spontaneous apneas and respiratory abnormalities during behavioral arousal in a mouse model of Rett syndrome. *Dis Model Mech* **7**, 1047–1055.

Kron M, Zimmermann JL, Dutschmann M, Funke F & Muller M (2011). Altered responses of MeCP2-deficient mouse brain stem to severe hypoxia. *J Neurophysiol* **105**, 3067–3079.

Lugaresi E, Cirignotta F & Montagna P (1985). Abnormal breathing in the Rett syndrome. *Brain Dev* **7**, 329–333.

Maezawa I & Jin LW (2010). Rett syndrome microglia damage dendrites and synapses by the elevated release of glutamate. *J Neurosci* **30**, 5346–5356.

Medrihan L, Tantalaki E, Aramuni G, Sargsyan V, Dudanova I, Missler M & Zhang W (2008). Early defects of GABAergic synapses in the brain stem of a MeCP2 mouse model of Rett syndrome. *J Neurophysiol* **99**, 112–121.

Moerschel M & Dutschmann M (2009). Pontine respiratory activity involved in inspiratory/expiratory phase transition. *Philos Trans R Soc Lond B Biol Sci* **364**, 2517–2526.

Morton RE, Bonas R, Minford J, Kerr A & Ellis RE (1997). Feeding ability in Rett syndrome. *Dev Med Child Neurol* **39**, 331–335.

Morton RE, Pinnington L & Ellis RE (2000). Air swallowing in Rett syndrome. *Dev Med Child Neurol* **42**, 271–275.

Okabe Y, Takahashi T, Mitsumasu C, Kosai K, Tanaka E & Matsuishi T (2012). Alterations of gene expression and glutamate clearance in astrocytes derived from an MeCP2-null mouse model of Rett syndrome. *PLoS One* **7**, e35354.

Paton JFR (1995). A working heart-brain-stem preparation of the mature mouse. *J Physiol* **489.P**, 155P–155P.

Paton JF & Kasparov S (1999). Differential effects of angiotensin II on cardiorespiratory reflexes mediated by nucleus tractus solitarii – a microinjection study in the rat. *J Physiol* **521**, 213–225.

Ramirez JM, Ward CS & Neul JL (2013). Breathing challenges in Rett syndrome: lessons learned from humans and animal models. *Respir Physiol Neurobiol* **189**, 280–287.

Ren J, Ding X, Funk GD & Greer JJ (2012). Anxiety-related mechanisms of respiratory dysfunction in a mouse model of Rett syndrome. *J Neurosci* **32**, 17230–17240.

Richter DW, Manzke T, Wilken B & Ponimaskin E (2003). Serotonin receptors: guardians of stable breathing. *Trends Mol Med* **9**, 542–548.

Schmid K, Foutz AS & Denavit-Saubie M (1996). Inhibitions mediated by glycine and $GABA_A$ receptors shape the discharge pattern of bulbar respiratory neurons. *Brain Res* **710**, 150–160.

Schreihofer AM, Stornetta RL & Guyenet PG (1999). Evidence for glycinergic respiratory neurons: Botzinger neurons express mRNA for glycinergic transporter 2. *J Comp Neurol* **407**, 583–597.

Song G, Tin C, Giacometti E & Poon CS (2011). Habituation without NMDA receptor-dependent desensitization of Hering-Breuer apnea reflex in a Mecp2 mutant mouse model of Rett syndrome. *Front Integr Neurosci* **5**, 6.

Song G, Wang H, Xu H & Poon CS (2012). Kolliker-Fuse neurons send collateral projections to multiple hypoxia-activated and nonactivated structures in rat brainstem and spinal cord. *Brain Struct Funct* **217**, 835–858.

Stettner GM, Huppke P, Brendel C, Richter DW, Gartner J & Dutschmann M (2007). Breathing dysfunctions associated with impaired control of postinspiratory activity in *Mecp2*$^{-/y}$ knockout mice. *J Physiol* **579**, 863–876.

Stettner GM, Zanella S, Hilaire G & Dutschmann M (2008*a*). 8-OH-DPAT suppresses spontaneous central apneas in the C57BL/6 J mouse strain. *Respir Physiol Neurobiol* **161**, 10–15.

Stettner GM, Zanella S, Huppke P, Gartner J, Hilaire G & Dutschmann M (2008*b*). Spontaneous central apneas occur in the C57BL/6 J mouse strain. *Respir Physiol Neurobiol* **160**, 21–27.

Stornetta RL, Rosin DL, Wang H, Sevigny CP, Weston MC & Guyenet PG (2003). A group of glutamatergic interneurons expressing high levels of both neurokinin-1 receptors and somatostatin identifies the region of the pre-Botzinger complex. *J Comp Neurol* **455**, 499–512.

Tan W, Pagliardini S, Yang P, Janczewski WA & Feldman JL (2010). Projections of preBotzinger complex neurons in adult rats. *J Comp Neurol* **518**, 1862–1878.

Toward MA, Abdala AP, Knopp SJ, Paton JF & Bissonnette JM (2013). Increasing brain serotonin corrects $CO_2$ chemosensitivity in methyl-CpG-binding protein 2 (Mecp2)-deficient mice. *Exp Physiol* **98**, 842–849.

Viemari JC, Roux JC, Tryba AK, Saywell V, Burnet H, Pena F, Zanella S, Bevengut M, Barthelemy-Requin M, Herzing LB, Moncla A, Mancini J, Ramirez JM, Villard L & Hilaire G (2005). Mecp2 deficiency disrupts norepinephrine and respiratory systems in mice. *J Neurosci* **25**, 11521–11530.

Voituron N & Hilaire G (2011). The benzodiazepine Midazolam mitigates the breathing defects of Mecp2-deficient mice. *Respir Physiol Neurobiol* **177**, 56–60.

Voituron N, Menuet C, Dutschmann M & Hilaire G (2010). Physiological definition of upper airway obstructions in mouse model for Rett syndrome. *Respir Physiol Neurobiol* **173**, 146–156.

Voituron N, Zanella S, Menuet C, Dutschmann M & Hilaire G (2009). Early breathing defects after moderate hypoxia or hypercapnia in a mouse model of Rett syndrome. *Respir Physiol Neurobiol* **168**, 109–118.

Yamashita Y, Matsuishi T, Ishibashi M, Kimura A, Onishi Y, Yonekura Y & Kato H (1998). Decrease in benzodiazepine receptor binding in the brains of adult patients with Rett syndrome. *J Neurol Sci* **154**, 146–150.

Yasui DH, Xu H, Dunaway KW, Lasalle JM, Jin LW & Maezawa I (2013). MeCP2 modulates gene expression pathways in astrocytes. *Mol Autism* **4**, 3.

Yokota S, Tsumori T, Oka T, Nakamura S & Yasui Y (2008). GABAergic neurons in the ventrolateral subnucleus of the nucleus tractus solitarius are in contact with Kolliker-Fuse nucleus neurons projecting to the rostral ventral respiratory group and phrenic nucleus in the rat. *Brain Res* **1228**, 113–126.

Zhang X, Su J, Cui N, Gai H, Wu Z & Jiang C (2011). The disruption of central CO2 chemosensitivity in a mouse model of Rett syndrome. *Am J Physiol Cell Physiol* **301**, C729–738.

## Additional information

### Competing interests

The authors have no competing interests to disclose.

### Author contributions

All experiments were performed at the University of Bristol. A.P.A. and J.M.B. conceived and designed the experiments. M.T. performed histological analysis in *Mecp2*$^{+/-}$-GAD$_{67}$-eGFP knock-in hybrid mice. A.P.A. performed all the *in situ* experiments. A.P.A., J.M.B., M.D. and J.F.R.P. assembled, analysed and interpreted the data. APA drafted the article. All authors revised the article critically for important intellectual content. All authors have approved the final version of the manuscript and agree to be accountable for all aspects of the work. All persons designated as authors qualify for authorship, and all those who qualify for authorship are listed.

### Funding

We are grateful to the International Rett Syndrome Foundation (2825), to the NewLife Foundation for Disabled Children (10-11/06) and to the National Institute of Neurological Disorders and Stroke, National Institutes of Health (NIH-NINDS, R01 NS069220) and the Rett Syndrome Research Trust for financial support.